Acta Neurochirurgica (2024) 166:359
https://doi.org/10.1007/s00701-024-06246-0

TECHNICAL NOTE

Evaluation of micro-remnant niduses of arteriovenous malformations post-gamma knife radiosurgery by 3D-rotational angiography

Ryuichi Noda[1,2] · Atsuya Akabane[1] · Mariko Kawashima[1] · Masafumi Segawa[2] · Sho Tsunoda[2] · Hiroyuki Wada[3] · Makoto Watanabe[3] · Haruyasu Yamada[3] · Tomohiro Inoue[2]

Received: 13 February 2024 / Accepted: 19 August 2024

Abstract

Purpose Recent innovations in radiological imaging have enabled the detection of micro-remnant niduses of arteriovenous malformations (AVMs) after gamma knife radiosurgery (GKS), which have not been previously perceptible. Herein, we focus on the difficulty of evaluating micro-remnant AVMs after GKS that are hardly perceptible on conventional examinations and propose integrating follow-up three-dimensional rotational angiography (3D-RA) in the previous gamma plan as a solution.

Methods We retrospectively searched NTT Medical Center Tokyo hospital database for patients with AVMs who underwent both two-dimensional digital subtraction angiography (2D-DSA) and 3D-RA as follow-up for GKS from February 2021 to January 2024. Patients with suspected nidus occlusion on the latest non-contrast-enhanced magnetic resonance angiography (NC-MRA) were included, and contrast-enhanced magnetic resonance angiography (CE-MRA), 2D-DSA, and 3D-RA were evaluated.

Results Twelve patients with 13 AVM sites were defined as having complete nidus occlusion on upfront NC-MRA. On 2D-DSA, seven AVM sites showed the presence of slight remaining AVMs based on the detection of remnant drainage veins, however the nidus was not detected in three cases. Nevertheless, 3D-RA detected micro-remnant niduses in all seven AVM sites, and four patients underwent re-GKS. Nine patients with ten AVM sites also underwent CE-MRA, and six AVM sites were diagnosed with radiation-induced parenchymal injury.

Conclusion Importing the 3D-RA image into the treatment planning has the potential to be more helpful than NC-MRA or CE-MRA to detect micro-remnant AVMs and evaluate the true remnant volume, and may contribute to a more detailed treatment planning, thereby improving the results of GKS retreatment.

Keywords Three-dimensional rotational angiography · Gamma knife · Remnant micro-arteriovenous malformations · Retreatment · Radiation-induced parenchymal injury

Introduction

Gamma knife radiosurgery (GKS) is an established modality for obliterating brain arteriovenous malformations (AVMs) [19]. A recent systematic review of 35 reports of 5,450 patients by China et al. reported an angiographically confirmed overall obliteration rate of 56.7% [5]. The obliteration rate has been in the spotlight, whereas the details of incomplete obliteration have never been meticulously examined. It is presumed that several degrees of remnant AVMs were included in this group, along with the smallest micro-remnant AVMs. In general, AVMs with a nidus of ≤ 1 cm are difficult to identify. Yasargil differentiated these from angiographically occult AVMs by defining them as micro-AVMs [36]. The diagnosis of remnant AVMs of this size range may be challenging because the diagnostic ability of computed tomography and magnetic resonance imaging (MRI) is not reliable in terms of spatial resolution [17], and even conventional two-dimensional digital subtraction angiography (2D-DSA) might show questionable findings or subtle abnormal findings, which

✉ Ryuichi Noda
rnrn46_8447@yahoo.co.jp

[1] Gamma Knife Center, NTT Medical Center Tokyo, Shinagawa-Ku, Tokyo, Japan

[2] Department of Neurosurgery, NTT Medical Center Tokyo, Shinagawa-Ku, Tokyo, Japan

[3] Department of Radiology, NTT Medical Center Tokyo, Shinagawa-Ku, Tokyo, Japan

Published online: 03 September 2024

can be easily overlooked by physicians [3]. Thus, a high index of suspicion is required to detect a micro-remnant AVM, particularly among post-radiosurgical lesions.

From another perspective, it is possible that the smallest remnant AVMs were customarily included in the complete obliteration group. For cases in which digital subtraction angiography (DSA) was not feasible for certain reasons, the decision about obliteration could have been made based on negative findings from follow-up MRIs. The lower image resolution of diagnostic radiological examinations in preceding generations could also have caused the underestimation of micro-remnant AVMs and resulted in their being defined as completely obliterated. The absence of differences between the arterial feeders and draining veins, both in terms of caliber and anatomical course, may hinder early venous filling, which is essential for the detection of micro-remnant shunts on 2D-DSA. Thus, the diagnosis of micro-remnant AVMs can be challenging because their manifestations on conventional 2D-DSA may be subtle or even presumed to be initially negative. Owing to these radiological characteristics, a near-complete obliterated nidus can be interpreted as a total occlusion, with the possibility of eventual rebleeding [10]. Therefore, the smallest remnant nidus should be properly detected and treated.

In this study, we focus on evaluating slight remnant niduses of AVMs after GKS that are hardly perceptible on MRI or 2D-DSA and propose a solution by demonstrating the usefulness of integrating follow-up three-dimensional rotational angiography (3D-RA) in the initial treatment plan, which may also be practical for the possible subsequent GKS retreatment.

Materials and methods

Ethics statements

Written informed consent was obtained from all patients, and the study protocol was approved by the local institutional review board (approval number: 000200000816–01).

Study design and population

In this study, we retrospectively searched our hospital database from February 2021 to January 2024 for patients who underwent DSA after GKS for AVM. Those who had both 2D-DSA and 3D-RA and who were suspected of having achieved nidus occlusion on non-contrast-enhanced magnetic resonance angiography (NC-MRA), were selected for the study.

Data collection and imaging

Data on the background characteristics, treatment courses, and radiological features of each patient were collected from an institutional review board-approved registry. All images, including NC-MRA, contrast-enhanced magnetic resonance angiography (CE-MRA), 2D-DSA, and 3D-RA, were meticulously analyzed by two neurosurgeons specializing in radiosurgery and a neurosurgeon specializing in neuro-interventional therapy. All NC-MRA and CE-MRA images were double-checked by radiologists.

The interval for follow-up MRIs was set to 6 or 12 months. The latest follow-up MRI images were acquired using 1.5-T (SIGNA Artist; GE Healthcare) or 3.0-T MRI scanners (Ingenia, Achieva; Philips Healthcare), whereas MRI images for GKS retreatment were acquired using 1.5-T MRI scanners (SIGNA Artist, Optima MR450w; GE Healthcare). Parameters of time-of-flight magnetic resonance angiography were as follows: SIGNA Artist: matrix size, 320×320 pixels; field of view, 200×200 mm^2; spatial resolution, 0.63×0.63 mm^2; and slice thickness, 1.0 mm; Optima MR450w: matrix size, 224×320 pixels; field of view, 200×200 mm^2; spatial resolution, 0.90×0.63 mm^2; and slice thickness, 1.0–1.2 mm; Achieva: matrix size, 362×724 pixels; field of view, 217×217 mm^2; spatial resolution, 0.63×0.30 mm^2; and slice thickness, 1.0 mm; and Ingenia: matrix size, 260×508 pixels; field of view, 200×200 mm^2; spatial resolution, 0.77×0.40 mm^2; and slice thickness, 1.0–1.2 mm. The repetition time was varied through 20, 22, 25, and 27. The echo time 2.9, 3.0, 3.1, 3.2, 3.3, 3.45, and 3.46, and the flip angle 18 or 20 (Supplementary Table S1). Acquisition of CE-MRA images was initiated immediately after the injection of the contrast medium. Either gadobutrol (0.1 mL/kg) or gadoteridol (0.2 mL/kg) was used as the contrast medium and injected manually, followed by a simultaneous 10-mL saline injection.

Digital subtraction angiography was performed using a single-plane angiography system (Artis Q Ceiling; Siemens Healthcare). Images from 2D-DSA were inspected for remaining niduses, feeding arteries, and draining veins. In addition to conventional 2D-DSA, 3D-RA was performed using 5sDSA or 6sDyna4D (Siemens Healthcare). We acquired the datasets using 5-s 200° and 6-s 260° acquisition programs for 5sDSA and 6sDyna4D, respectively. The acquired images included the entire cranium for better image co-registration. The contrast medium (iomeprol, 300 mg iodine/mL) was injected with a power injector via a 4-French catheter inserted from the femoral artery, and the injection rate was determined individually, usually 2.0–4.5 mL/s, by the neuroendovascular surgeon (R.N.) based on the findings of 2D-DSA.

The total volume of contrast medium injected for a single acquisition was 12–24 mL. The volume dataset obtained was converted into computed tomography-like images with 512 × 512 × 512 voxels and a spatial resolution of 0.10–0.49 mm (Supplementary Table S2), then inspected by the Leksell Gamma Plan software (Elekta Instrument, Stockholm, Sweden) as multi planar reconstruction images. Images from 3D-RA were integrated with other follow-up MRI images into the previous treatment plan, co-registered with images from the previous treatment, and analyzed using Leksell Gamma Plan software. The remaining nidus volume was measured using Leksell Gamma Plan software on NC-MRA, CE-MRA, and 3D-RA images; lesions with volumes of ≤ 0.5 cc on 3D-RA images were defined as a micro-remnant nidus. The radiation-induced parenchymal injury was defined as the difference between the lesion on 3D-RA and that on CE-MRA.

Results

Nineteen patients with 20 AVM sites underwent follow-up DSA, along with 3D-RA of AVMs treated with GKS. Thirteen patients with 14 AVM sites were defined as having complete nidus occlusion on upfront NC-MRA. One patient was excluded because of a lack of previous GKS treatment data. Table 1 lists the baseline characteristics of the 12 patients with 13 AVM sites. Initial GKS was performed using Icon™ or Perfexion™ (Elekta Instrument).

The treatments were performed from 2012 to 2019, and all treatment plans were meticulously created and revised using the Leksell Gamma Plan software by the same senior physician. All AVM sites showed total obliteration on NC-MRA. Images of CE-MRA were available for ten AVM sites, and only two of them showed negative signs of a remnant lesion. However, both cases turned out to be false negatives according to the results of 2D-DSA and 3D-RA. Of the other eight AVM sites that showed a remnant lesion on CE-MRA, six showed an exaggeration of the contrast-enhanced lesion volume due to radiation-induced parenchymal injury. On 2D-DSA, seven AVM sites showed a remnant AVM, as detected by the remaining drainage vein. Among which, 2D-DSA failed to detect the remaining nidus in three cases. Consequently, seven AVM sites showed micro-remnant niduses on 3D-RA images. These results correspond to those of the draining vein on 2D-DSA. Three of the remaining small niduses were located within the irradiated field, with two coexisting radiation-induced parenchymal injuries. Four of the seven remnant lesions were due to the targeting error of the initial treatment. Additionally, there were four cases in which 3D-RA images revealed that the positive sign of a remnant nidus on CE-MRA was a false positive sign caused by radiation-induced parenchymal injury. Two AVM sites demonstrated exaggeration of the suspected nidus lesions on CE-MRA because of radiation-induced parenchymal injury. Finally, four patients underwent GKS retreatment for micro-remnant AVMs. The diagnoses of the 13 AVM sites were as follows: complete obliteration (AVM site 11 and 12), pure remnant lesion (AVM site 1; Fig. 1), remnant lesion due to a targeting error (AVM site 2, 3, 5, and 7; Fig. 2), remnant lesion with radiation-induced parenchymal injury (AVM site 4 and 6; Fig. 3), and pure radiation-induced parenchymal

Table 1 Baseline characteristics of the 13 AVM sites

Case No	AVM site	Age (y)	Sex	Presentation	Location	Size (mm)	Vol. (cc)	S-M (grade)	Rx dose (Gy)	Max dose (Gy)	GKS to OM (y)
1	1	33	M	R	OL	15×5×6	0.2	2	18	26.1	2
2	2	39	F	R	TL	12×9×7	0.5	2	20	27.8	4
3	3	24	F	I	PL	8×10×6	0.2	3	16	25.8	3
4	4	27	F	I	FL	31×22×37	14	2	14	20.0	8
5	5	41	F	R	OL	14×13×11	0.6	3	20	30.3	9
6	6	31	F	E	TL	17×12×14	1.3	2	16	26.2	3
7	7	20	M	R	CER	13×6×10	0.5	2	18	24.0	2
	8				CER	16×6×10	0.6	2	18	24.0	2
8	9	61	F	E	TL	25×20×24	4.9	1	18	26.1	2
9	10	24	F	R	TH	30×29×33	13.8	4	18	36.0	3
10	11	38	M	H	FL	17×17×13	2.5	2	18	27.3	2
11	12	22	F	R	PL	25×24×16	3.3	2	17	23.6	3
12	13	31	M	R	BS	12×16×15	0.7	2	18	26.9	2

Abbreviations: *BS* Brain stem, *CER* Cerebellum, *E* Epilepsy, *F* Female, *FL* Frontal lobe, *GKS* Gamma knife radiosurgery, *H* Headache, *I* Incidental, *M* Male, *No* Number, *OL* Occipital lobe, *OM* Obliteration on magnetic resonance imaging, *PL* Parietal lobe, *R* Rupture, *Rx* Prescribed, *S-M* Spetzler-Martin, *TL* Temporal lobe, *TH* Thalamus, *Vol* Volume, *y* Years

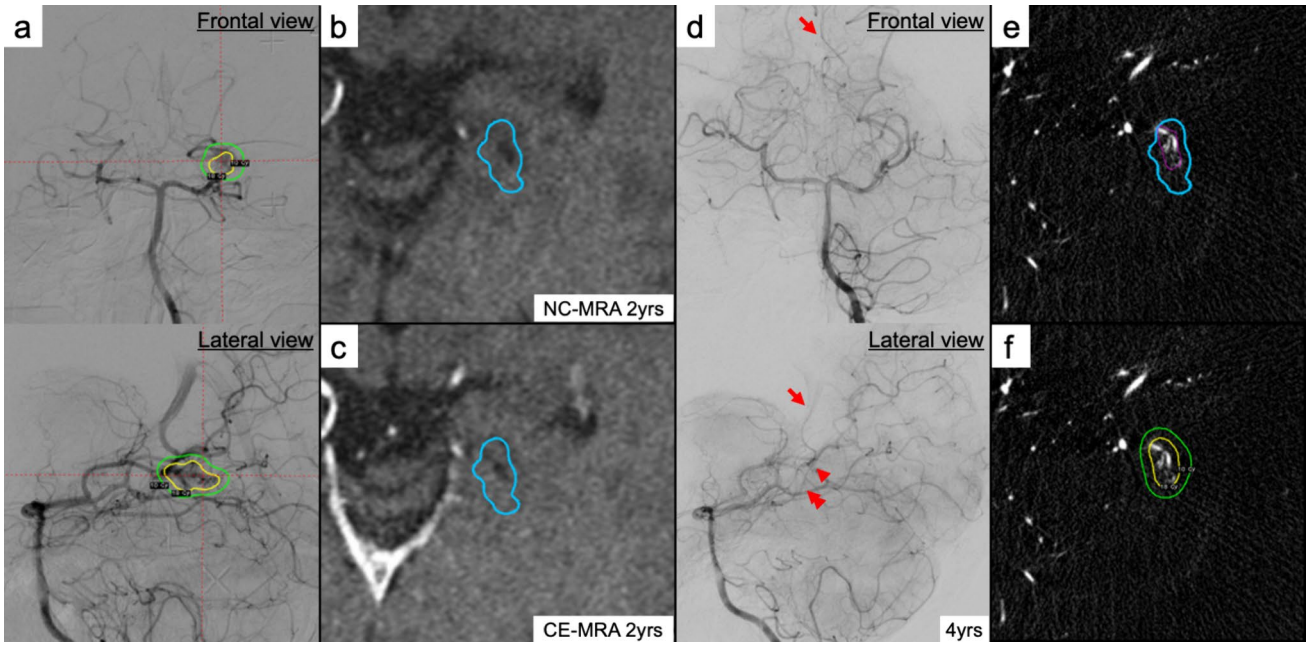

Fig. 1 Radiological images of case 1. A 28-year-old male underwent gamma knife surgery (GKS) for an arteriovenous malformation (AVM) of the occipital lobe that initially presented with intracranial hemorrhage. The treatment plan (15×5×6 mm, volume of 0.2 cc, prescription dose of 18 Gy, maximum dose of 26.1 Gy) for AVM (Spetzler-Martin grade 2) is demonstrated on two-dimensional digital subtraction angiography (2D-DSA). The feeding artery was the left posterior cerebral artery drained by the inferior sagittal sinus. (**a**, frontal and lateral views) Two years later, obliteration was suspected in non-contrast-enhanced magnetic resonance angiography (NC-MRA) (**b**, axial image) and contrast-enhanced magnetic resonance angiography (CE-MRA). (**c**, axial image) However, 2D-DSA performed 4 years after GKS demonstrated the existence of the remaining nidus (arrowhead), feeding artery (double arrowhead), and draining vein (arrow). (**d**, frontal and lateral views) Three-dimensional rotational angiography revealed the actual remnant nidus (pink line) within the previously irradiated field (blue line). The patient underwent retreatment with GKS (yellow and green lines indicate the 18-Gy and 10-Gy areas, respectively) of the micro-remnant nidus. (**e**, **f**, axial image) The patient exhibited a micro-remnant AVM due to incomplete obliteration after GKS

injury (AVM site 8, 9, 10 and 13). Table 2 presents the results for each imaging modality.

Discussion

Owing to recent progress in the field of neuroimaging, several radiological modalities have been considered as candidates for follow-up examination and as possible replacements for conventional DSA, which is considered invasive for follow-up examinations. The NC-MRA performed using the time-of-flight technique showed better sensitivity for nidus occlusion than for spin-echo imaging on follow-up MRI [14, 20]. However, in a report of 15 cases with micro-remnant AVMs, Mukherji et al. showed that the sensitivity and specificity were 50% and 100%, respectively [21]. The most noteworthy limitation of NC-MRA, which is critical for detecting micro-AVMs, is that faint flow signals may be underestimated on the image [1]. In our cases, NC-MRA was insufficiently sensitive to detect micro-remnant niduses. Therefore, if NC-MRA is negative, it should be followed-up with DSA (with or without 3D-RA) to make sure there is no residual shunting. However, due to its low invasiveness and accessibility, NC-MRA remains the first choice for follow-up examinations.

Time-of-flight CE-MRA images (including the time-resolved sequences) are considered to play an effective role in follow-up imaging after stereotactic radiosurgery for AVMs [7]. Lee et al. conducted a series of 32 AVMs with a mean volume of 2.3 (0.1–11.0) cm^3 treated by GKS. The diagnostic accuracy of CE-MRA during follow-up was 75–78%. The authors referred to the limitation of low spatial resolution, which might have caused an underestimation of the small remnant AVMs. Another limitation was that CE-MRA may have overestimated the remnant nidus by enhancing possible radiation-induced parenchymal injury [16]. Radiation-induced parenchymal injury after GKS of AVMs was first described by Yamamoto et al. [32] in 1992 and has been described in detail in subsequent publications [33, 34]. This was observed in 24% of patients in the chronic phase of post-stereotactic radiosurgery of AVMs and was correlated with higher nidus obliteration [18]. Radiation-induced parenchymal injury after GKS is usually observed on contrast-enhanced T1-weighted images with an irregular

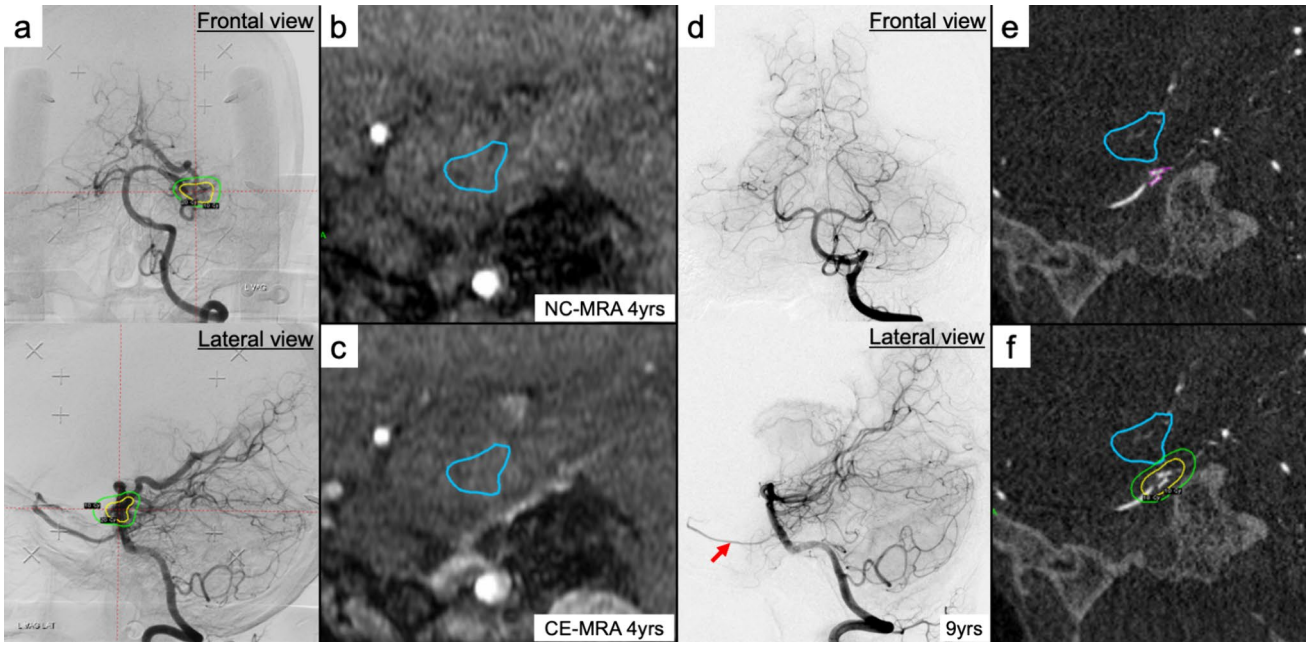

Fig. 2 Radiological images of case 2. A 29-year-old female who initially presented with intracranial hemorrhage was diagnosed with an arteriovenous malformation (AVM) (Spetzler-Martin grade 2) of the temporal lobe. The treatment plan (12×9×7 mm, 0.5 cc, prescription dose of 20 Gy, maximum dose of 27.8 Gy) of the AVM (Spetzler-Martin grade 2) was demonstrated on two-dimensional digital subtraction angiography (2D-DSA). The feeding arteries were the left posterior cerebral and left anterior choroidal arteries, and the draining veins were the basal vein of the Rosenthal and sphenoparietal sinus. (**a**, frontal and lateral views) Four years later, AVM obliteration is suspected on non-contrast-enhanced magnetic resonance angiography (NC-MRA) (**b**, sagittal image), and contrast-enhanced magnetic resonance angiography (CE-MRA) shows a negative sign. (**c**, sagittal image) Although 2D-DSA performed 9 years after gamma knife surgery (GKS) demonstrated an apparent drainage vein (arrow), (**d**, frontal and lateral views) three-dimensional rotational angiography images revealed the remnant nidus (pink line) outside the previously irradiated field (blue line). The patient underwent GKS retreatment (yellow and green lines indicate the 18-Gy and 10-Gy area, respectively) of the micro-remnant nidus. (**e**, **f**, sagittal image) The patient had a micro-remnant AVM due to a targeting error of the previous GKS

or nodular feature without vascular branching. Generally, subtraction of the time-of-flight NC-MRA image findings from the contrast-enhanced T1-weighted image findings can indicate radiation-induced parenchymal injury [16, 22]. However, we should be aware of the necessity of carefully differentiating nidus remnants from radiation-induced parenchymal injuries on CE-MRA images.In our series, CE-MRA images showed both underestimation and overestimation of micro-remnant AVM lesions. Nevertheless, combining several MRI sequences is essential to achieve a more accurate detection and evaluation of small AVM remnants. Leclerc et al. reviewed the diagnostic effectiveness of their series by combining multi-sequence MRI images, and the sensitivity and specificity were 75% and 100%, respectively [15]. Rojas-Villabona et al. reported that the combination of arterial spin-labeling MRA with contrast-enhanced time-resolved MRA was reliable for confirming the obliteration of post-GKS brain AVMs. However, they did not perform volumetric evaluation of the remnant lesions nor account for the possibility of radiation-induced parenchymal injuries [26].

DSA is the established gold standard for the follow-up examination of AVMs after GKS. Since CE-MRA images have a significantly lower spatial resolution than that of 2D-DSA images [31], conventional 2D-DSA has long been the standard imaging modality for follow-up after AVM treatment, despite its high invasiveness. The spatial resolution required to create a fine image and the temporal resolution necessary to study hemodynamics are indispensable. In our cases, 2D-DSA was more sensitive than CE-MRA in detecting the remaining draining vein. However, according to a case series, the diagnosis of micro-remnant niduses can be challenging because of the absence of obvious anatomical vascular abnormalities and increased hemodynamic blood flow [3]. These factors could hinder the recognition of early venous filling, which is key to the diagnosis, and may lead to false occlusion. Indeed, the remnant nidus was not detected based on some of our 2D-DSA results. As a matter of fact, it is impossible to make a detailed and meticulous comparison with the previous treatment plan using 2D-DSA images, although it is indispensable when considering GKS retreatment.

The use of 3D-RA in the field of GKS for treatment planning was first reported by Sagfain et al. in 2016 [27]. The authors reported preliminary results of integrating cone

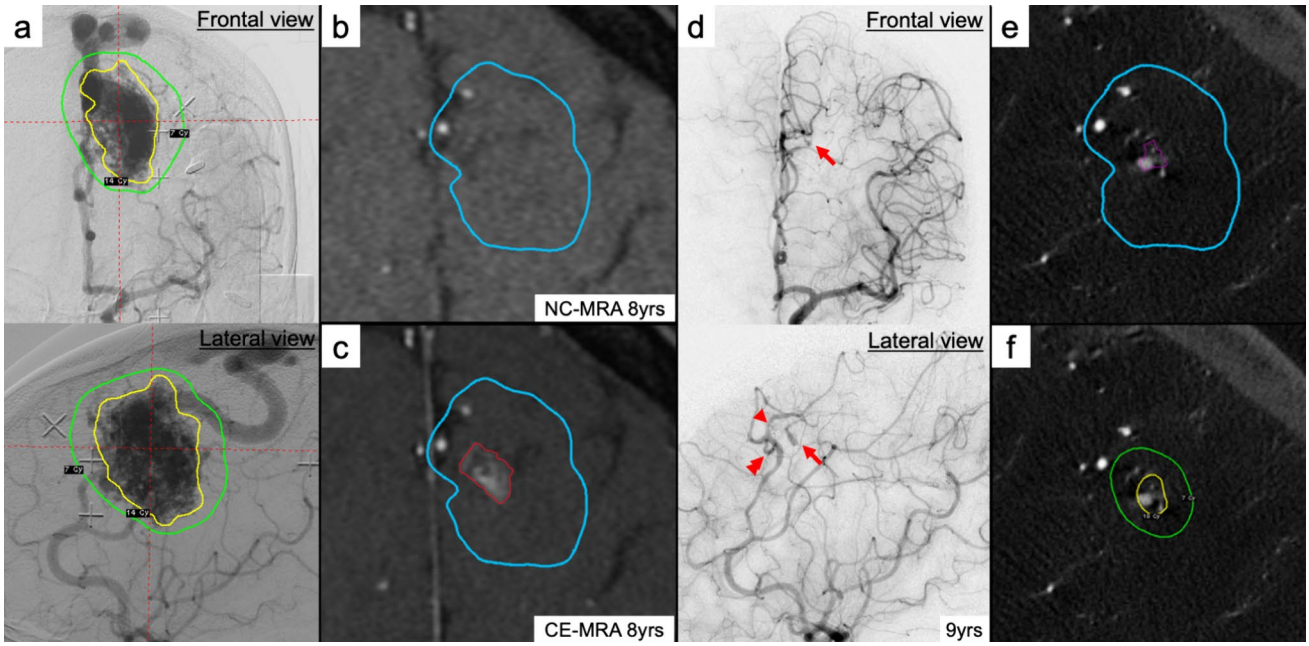

Fig. 3 Radiological images of case 4. An 18-year-old female underwent gamma knife surgery (GKS) for an incidentally diagnosed arteriovenous malformation (AVM) (Spetzler-Martin grade 2) of the frontal lobe. The treatment plan (31 × 22 × 37 mm, 14.0 cc, prescription dose of 14 Gy, maximum dose of 20.0 Gy) for AVM (Spetzler-Martin grade 2) is demonstrated on two-dimensional digital subtraction angiography (2D-DSA). The feeding artery was the left anterior cerebral artery drained by the cortical vein. (**a**, frontal and lateral views) Eight years later, although obliteration was suspected on non-contrast-enhanced magnetic resonance angiography (NC-MRA) (**b**, axial image), contrast-enhanced magnetic resonance angiography (CE-MRA) showed a positive sign for a remaining nidus (red line). (**c**, axial image) The 2D-DSA performed 9 years after GKS demonstrates the remaining nidus (arrowhead) with a feeding artery (double arrowhead) and draining vein (arrow). (**d**, frontal and lateral views) The remnant nidus that was revealed by 3D-RA (pink line) was within the previously irradiated field (blue line) and was significantly smaller than that on CE-MRA. The patient underwent retreatment with GKS (yellow and green lines indicate the 18-Gy and 10-Gy areas, respectively) of the micro-remnant nidus. (**e**, **f**, axial image) The patient had a micro-remnant AVM due to incomplete obliteration. Radiation-induced parenchymal injury exaggerated the true remnant lesion on CE-MRA

Table 2 Results of the follow-up radiological images

Case No	AVM site	GKS to 3D-RA	NC-MRA	CE-MRA	2D-DSA			3D-RA	Dx	Rx dose	Max dose
		(y)	Vol. (cc)	Vol. (cc)	F	N	D	Vol. (cc)		(Gy)	(Gy)
1	1	4	CO	CO	+	+	+	0.04	NR	18	25.7
2	2	9	CO	CO	−	−	+	0.004	TE	18	27.7
3	3	4	CO	0.1	−	−	+	0.1	TE	16	22.8
4	4	9	CO	0.6	+	+	+	0.08	NR/RPI	18	22.5
5	5	9	CO	N/A	−	−	+	0.002	TE	-	-
6	6	4	CO	0.1	+	+	+	0.05	NR/RPI	-	-
7	7	3	CO	0.6	+	+	+	0.5	TE	-	-
	8		CO	0.06	−	−	−	CO	RPI	-	-
8	9	4	CO	0.2	−	−	−	CO	RPI	-	-
9	10	4	CO	0.8	−	−	−	CO	RPI	-	-
10	11	4	CO	N/A	−	−	−	CO	CO	-	-
11	12	9	CO	N/A	−	−	−	CO	CO	-	-
12	13	9	CO	0.02	−	−	−	CO	RPI	-	-

Abbreviations: *2D-DSA* Two-dimensional digital subtraction angiography, 3D-RA three-dimensional rotational angiography, *CE-MRA* Contrast-enhanced magnetic resonance angiography, *CO* Complete obliteration, *D* Draining vein, *Dx* Diagnosis, *F* Feeding artery, *GKS* Gamma knife radiosurgery, *N* Nidus, *N/A* Not available, *NC-MRA* Non-contrast-enhanced magnetic resonance angiography, *No* Number, *NR* Remnant nidus, *RPI* Radiation-induced parenchymal injury, *Rx* Prescribed, *TE* Targeting error. *Vol* Volume

beam computed tomography with conventional 2D-DSA into the gamma plan. The following studies have demonstrated the effectiveness of integrating 3D-RA in treatment planning [4, 11–13, 28, 29]. Furthermore, it is noteworthy that the dose for 5s3D-RA was found to be slightly less when compared to a standard 2D-DSA (0.9 mSv versus. 1 mSv) [30]. Colombo et al. referred to the possibility of using 3D-RA as a follow-up method in the LINAC series. Fusing the 3D-RA images with the stereotactic images used in the treatment plan will allow accurate evaluation of the smallest remnant [6]. Hasegawa et al. demonstrated an illustrative case of a retreated faint remnant AVM after GKS detection by 3D-RA [11]. However, we are the first to demonstrate the effectiveness of 3D-RA in detecting and evaluating micro-remnant niduses of treated AVMs and differentiating them from radiation-induced parenchymal injury. This modality will not only detect the slightest remaining nidus unseen on MRI but will also help elucidate the cause of incomplete treatment results, such as targeting errors, by integrating the 3D-RA follow-up images with the previous treatment plan data. In addition, spatial and contrast resolution may be further increased with longer rotations and higher number of projections, but this results in approximately higher radiation exposure compared to conventional 3D-RA (20sDynaCT; 2.9 mSv versus 5sDSA; 0.9 mSv) [25, 27, 30]. The radiation exposure of 6sDyna4D, used in our series, was supposed to be still lower than 20sDynaCT, since the required number of frames for this image acquisition was 173, compared to 133 for 5sDSA (Supplementary Table S2). It may be worthwhile to occasionally apply this technique for treatment planning, as Hasegawa et al. described [12]; however, we consider it relatively excessive for routine use in simple follow-up angiography.

According to several analyses of treatment failure after radiosurgery, one of the most frequent treatment failures is a targeting error [8, 9, 24, 35], especially when the initial treatment is performed with reference to a lower-resolution image for technical reasons. Accordingly, considering the possibility of repeated radiosurgery, it is crucial to elucidate whether the remnant nidus, especially when it is small, is located within the irradiated field. Indeed, more than half of our micro-remnant AVMs were due to a targeting error. A systematic review of 14 studies with 733 patients reported that micro-remnant AVMs can undergo repeat radiosurgery with an occlusion rate of 61% with risks of hemorrhage and radiation-induced changes of 7.6% and 7.4%, respectively [2]. A recent publication from a single institution reported that in 170 patients with retreated AVMs, the occlusion rates were 37.6%, 57.3%, and 80.9% at 3, 5, and 10 years, respectively. In that report, hemorrhage and symptomatic radiation-induced changes occurred in 8.2% and 8.8% of patients, respectively [23]. In retreatment cases, the obliteration rate was lower or the occlusion process seemed to take longer than those in treatment-naïve lesions. In addition, the complication rate seemed to be high compared with the results of the first treatment. This may be due to the technical limitations of conventional treatment performed without the integration of 3D-RA into the treatment plan. Thus, it is essential to delineate the remnant lesion and its relationship to the initially irradiated lesion to provide safe and effective treatment.

This study has a couple of limitations. First, since this was a study involving a small population from a single institute, the results are limited in generalizability; thus, further research with more patients from multiple institutions is required. Second, because the outcomes of the four retreated cases have not been elucidated yet, further accumulation of cases and comparison with conventional retreatment results are required. However, with the accurate differentiation of the smallest target from radiation-induced parenchymal injury by finely delineating the remnant nidus, the risk of retreatment is estimated to be minimal.

Conclusions

According to our series, NC-MRA images are insufficiently sensitive or selective for detecting micro-remnant niduses of AVMs after GKS. Even with the use of contrast enhancement, MRI images may underestimate the remaining lesion or even overestimate it by demonstrating radiation-induced parenchymal injury; thus, merely using contrast enhancement should not be the last resort for the follow-up imaging. We also found that 2D-DSA was more sensitive than CE-MRA in detecting the remaining AVM by demonstrating the residual draining vein, however it was insufficient to evaluate the detailed location and volume of the micro-remnant nidus. Importing the 3D-RA image into the gamma plan accurately delineates the remnant lesion and avoids waste radiation exposure to the previously irradiated area, which subsequently leads to effective and safe treatment. Accordingly, this preliminary report shows that 2D-DSA/3D-RA is indispensable for confirming nidus obliteration and contributes to improving the treatment results of GKS retreatment of micro-remnant AVMs. Even if NC-MRA is negative, CE-MRA should not be considered as an alternative to 3D-RA, as CE-MRA images showed both underestimation (two out of ten AVM sites) and overestimation (six out of ten AVM sites) of micro-remnant AVM lesions in our series. Instead, it should be followed-up with 2D-DSA, and with additional 3D-RA if there is any suspected sign of remnant lesion. In addition, the 3D-RA should be imported to the previous treatment plan and analyzed using Leksell Gamma Plan software. To the best of our knowledge, this is the first report to demonstrate the utility of DSA, including 3D-RA, as a follow-up modality. Although this study had a small sample size, we believe that the results will be a convincing aid to

encourage the indication of DSA as a follow-up examination, especially for patients who are reluctant to undergo stressful, invasive procedures. If retreatment is required, the 3D-RA images can be integrated into the retreatment planning so that the patient does not have to undergo another DSA on the day of the GKS procedure.

Supplementary Information The online version contains supplementary material available at https://doi.org/10.1007/s00701-024-06246-0.

Acknowledgements The authors thank Siemens Healthineers Japan for technical information of the single-plane angiography system (Artis Q ceiling)

Author contributions Ryuichi Noda: Conceptualization, data curation, investigation, methodology, visualization, and writing of the original draft.

Atsuya Akabane: Writing – review and editing, data curation, supervision, software, project administration, validation, investigation.

Mariko Kawashima: Data curation, investigation, methodology, software, validation, and writing – review and editing (lead).

Masafumi Segawa: Investigation, validation, and writing – review and editing.

Sho Tsunoda: Investigation and writing – review and editing.

Hiroyuki Wada: Data curation, software, visualization.

Makoto Watanabe: Data curation, software, visualization.

Haruyasu Yamada: Supervision, validation, and writing – review and editing.

Tomohiro Inoue: Project administration, resources, supervision, validation,

writing – review and editing.

Funding The authors declare that no funds, grants, or other support were received during the preparation of this manuscript.

Data availability The author confirms that the data supporting the findings of this study are available within the article and its supplementary materials.

Declarations

Conflict of interest The authors have no relevant financial or non-financial interests to disclose.

Ethical approval This retrospective chart review study involving human participants was conducted in accordance with the ethical standards of the institutional and national research committee and with the 1964 Helsinki Declaration and its later amendments or comparable ethical standards. The Human Investigation Committee (IRB) of NTT Medical Center Tokyo approved this study (approval No.: 000200000816–01).

Consent to publish The authors affirm that human research participants provided informed consent for publication of the images in all figures.

References

1. Anderson CM, Saloner D, Tsuruda JS, Shapeero LG, Lee RE (1990) Artifacts in maximum-intensity-projection display of MR angiograms. AJR Am J Roentgenol 154:623–629. https://doi.org/10.2214/ajr.154.3.2106232
2. Awad AJ, Walcott BP, Stapleton CJ, Ding D, Leed CC, Loeffler JS (2015) Repeat radiosurgery for cerebral arteriovenous malformations. J Clin Neurosci 22:945–950. https://doi.org/10.1016/j.jocn.2015.01.015
3. Cellerini M, Mangiafico S, Villa G, Nistri M, Pandolfo C, Noubari H, Ammannati F, Mennonna P, Scollato A, Perrini P, Di Lorenzo N, Giordano GP (2002) Cerebral microarteriovenous malformations: diagnostic and therpeutic features in a series of patients. AJNR Am J Neuroradiol 23:945–952
4. Chen KK, Guo WY, Yang HC, Lin CJ, Wu CF, Gehrisch S, Kowarschik M, Wu YT, Chung WY (2017) Application of time-resolved 3D digital subtraction angiography to plan cerebral arteriovenous malformation radiosurgery. AJNR Am J Neuroradiol 38:740–746. https://doi.org/10.3174/ajnr.A5074
5. China M, Vastani A, Hill CS, Tancu C, Grover PJ (2022) Gamma knife radiosurgery for cerebral arteriovenous malformations: a systematic review and meta-analysis. Neurosurg Rev 45:1987–2004. https://doi.org/10.1007/s10143-022-01751-1
6. Colombo F, Cavedon C, Francescon P, Casentini L, Fornezza U, Castellan L, Causin F, Perini S (2003) Three-dimensional angiography for radiosurgical treatment planning for arteriovenous malformations. J Neurosurg 98:536–543. https://doi.org/10.3171/jns.2003.98.3.0536
7. Duran M, Schoenberg SO, Yuh WT, Knopp MV, van Kaick G, Essig M (2002) Cerebral arteriovenous malformations: morphologic evaluation by ultrashort 3D gadolinium-enhanced MR angiography. Eur Radiol 12:2957–2964. https://doi.org/10.1007/s00330-002-1418-y
8. Ellis TL, Friedman WA, Bova FJ, Kubilis PS, Buatti JM (1998) Analysis of treatment failure after radiosurgery for arteriovenous malformations. J Neurosurg 89:104–110. https://doi.org/10.3171/jns.1998.89.1.0104
9. Gallina P, Merienne L, Meder JF, Schlienger M, Lefkopoulos D, Merland JJ (1998) Failure in radiosurgery treatment of cerebral arteriovenous malformations. Neurosurgery 42:996–1002; discussion 1002–1004. https://doi.org/10.1097/00006123-199805000-00024.
10. Guo WY, Karlsson B, Ericson K, Lindqvist M (1993) Even the smallest remnant of an AVM constitutes a risk of further bleeding. Case report Acta Neurochir (Wien) 121:212–215. https://doi.org/10.1007/BF01809278
11. Hasegawa H, Hanakita S, Shin M, Kawashima M, Kin T, Takahashi W, Shojima M, Nomoto AK, Aoki S, Saito N (2018) Integrating 3D rotational angiography into gamma knife planning. AJNR Am J Neuroradiol 39:1867–1870. https://doi.org/10.3174/ajnr.A5763
12. Hasegawa H, Hanakita S, Shin M, Kawashima M, Kin T, Takahashi W, Suzuki Y, Shinya Y, Ono H, Shojima M, Nakatomi H, Saito N (2018) Integration of rotational angiography enables better dose planning in gamma knife radiosurgery for brain arteriovenous malformations. J Neurosurg 129:17–25. https://doi.org/10.3171/2018.7.GKS181565
13. Kang J, Huang J, Gailloud P, Rigamonti D, Lim M, Bernard V, Ehtiati T, Ford EC (2014) Planning evaluation of C-arm cone beam CT angiography for target delineation in stereotactic radiation surgery of brain arteriovenous malformations. Int J Radiat Oncol Biol Phys 90:430–437. https://doi.org/10.1016/j.ijrobp.2014.05.035
14. Kauczor HU, Engenhart R, Layer G, Gamroth AH, Wowra B, Schad LR, Semmler W, van Kaick G (1993) 3D TOF MR angiography of cerebral arteriovenous malformations after radiosurgery. J Comput Assist Tomogr 17:184–190. https://doi.org/10.1097/00004728-199303000-00005
15. Leclerc X, Guillaud O, Reyns N, Hodel J, Outteryck O, Bala F, Bricout N, Bretzner M, Ramdane N, Pruvo JP, Hacein-Bey L,

Kuchcinski G (2020) Follow-up MRI for small brain AVMs treated by radiosurgery: is gadolinium really necessary? AJNR Am J Neuroradiol 41:437–445. https://doi.org/10.3174/ajnr.A6404
16. Lee KE, Choi CG, Choi JW, Choi BS, Lee DH, Kim SJ, Kwon DH (2009) Detection of residual brain arteriovenous malformations after radiosurgery: diagnostic accuracy of contrast-enhanced three-dimensional time of flight MR angiography at 3.0 Tesla. Korean J Radiol 10:333–339. https://doi.org/10.3348/kjr.2009.10.4.333
17. Lee CC, Reardon MA, Ball BZ, Chen CJ, Yen CP, Xu Z, Wintermark M, Sheehan J (2015) The predictive value of magnetic resonance imaging in evaluating intracranial arteriovenous malformation obliteration after stereotactic radiosurgery. J Neurosurg 123:136–144. https://doi.org/10.3171/2014.10.JNS141565
18. Lunsford LD, Kondziolka D, Bissonette DJ, Maitz AH, Flickinger JC (1992) Stereotactic radiosurgery of brain vascular malformations. Neurosurg Clin N Am 3:79–98. https://doi.org/10.1016/S1042-3680(18)30684-3
19. Maruyama K, Kawahara N, Shin M, Tago M, Kishimoto J, Kurita H, Kawamoto S, Morita A, Kirino T (2005) The risk of hemorrhage after radiosurgery for cerebral arteriovenous malformations. N Engl J Med 352:146–153. https://doi.org/10.1056/NEJMoa040907
20. Morikawa M, Numaguchi Y, Rigamonti D, Kuroiwa T, Rothman MI, Zoarski GH, Simard JM, Eisenberg H, Amin PP (1996) Radiosurgery for cerebral arteriovenous malformations: assessment of early phase magnetic resonance imaging and significance of gadolinium-DTPA enhancement. Int J Radiat Oncol Biol Phys 34:663–675. https://doi.org/10.1016/0360-3016(95)02160-4
21. Mukherji SK, Quisling RG, Kubilis PS, Finn JP, Friedman WA (1995) Intracranial arteriovenous malformations: quantitative analysis of magnitude contrast MR angiography versus gradient-echo MR imaging versus conventional angiography. Radiology 196:187–193. https://doi.org/10.1148/radiology.196.1.7784565
22. Nataf F, Ghossoub M, Missir O, Merienne L, Roux FX, Meder JF, Trystram D, Schlienger M, Merland JJ, Chodkiewicz JP (1997) Parenchymal changes after radiosurgery of cerebral arteriovenous malformations. Preliminary report of a proposed classification. Stereotact Funct Neurosurg 69:143–146. https://doi.org/10.1159/000099866
23. Pikis S, Mantziaris G, Ramanathan P, Xu Z, Sheehan JP (2022) Repeat stereotactic radiosurgery for cerebral arteriovenous malformations. Neurosurg Focus 53:E11. https://doi.org/10.3171/2022.4.FOCUS2294
24. Pollock BE, Kondziolka D, Lunsford LD, Bissonette D, Flickinger JC (1996) Repeat stereotactic radiosurgery of arteriovenous malformations: factors associated with incomplete obliteration. Neurosurgery 38:318–324. https://doi.org/10.1097/00006123-199602000-00016
25. Rahal JP, Malek AM (2013) Benefit of cone-beam computed tomography angiography in acute management of angiographically undetectable ruptured arteriovenous malformations. J Neurosurg 119:1015–1020. https://doi.org/10.3171/2013.4.JNS1390
26. Rojas-Villabona A, Pizzini FB, Solbach T, Sokolska M, Ricciardi G, Lemonis C, DeVita E, Suzuki Y, van Osch MJP, Foroni RI, Longhi M, Montemezzi S, Atkinson D, Kitchen N, Nicolato A, Golay X, Jäger HR (2021) Are Dynamic Arterial Spin-Labeling MRA and Time-Resolved Contrast-Enhanced MRA Suited for Confirmation of Obliteration following Gamma Knife Radiosurgery of Brain Arteriovenous Malformations? AJNR Am J Neuroradiol 42:671–678. https://doi.org/10.3174/ajnr.A6990
27. Safain MG, Rahal JP, Raval A, Rivard MJ, Mignano JE, Wu JK, Malek AM (2014) Use of cone-beam computed tomography angiography in planning for gamma knife radiosurgery for arteriovenous malformations: a case series and early report. Neurosurgery 74:682–695; discussion 695–696. https://doi.org/10.1227/NEU.0000000000000331
28. Shinya Y, Hasegawa H, Shin M, Kawashima M, Sugiyama T, Ishikawa O, Koizumi S, Suzuki Y, Nakatomi H, Saito N (2021) Rotational angiography-based gamma knife radiosurgery for brain arteriovenous malformations: preliminary therapeutic outcomes of the novel method. Neurosurgery 89:60–69. https://doi.org/10.1093/neuros/nyab066
29. Shinya Y, Hasegawa H, Kawashima M, Koizumi S, Katano A, Umekawa M, Saito N (2023) Prognosis of rotational angiography-based stereotactic radiosurgery for dural arteriovenous fistulas: a retrospective analysis. Neurosurgery 92:167–178. https://doi.org/10.1227/neu.0000000000002168
30. Struffert T, Hauer M, Banckwitz R, Köhler C, Royalty K, Doerfler A (2014) Effective dose to patient measurements in flat-detector and multislice computed tomography: a comparison of applications in neuroradiology. Eur Radiol 24(6):1257–1265. https://doi.org/10.1007/s00330-014-3136-7
31. Unlu E, Temizoz O, Albayram S, Genchellac H, Hamamcioglu MK, Kurt I, Demir MK (2006) Contrast-enhanced MR 3D angiography in the assessment of brain AVMs. Eur J Radiol 60:367–378. https://doi.org/10.1016/j.ejrad.2006.08.007
32. Yamamoto M, Jimbo M, Kobayashi M, Toyoda C, Ide M, Tanaka N, Lindquist C, Steiner L (1992) Long-term results of radiosurgery for arteriovenous malformation: neurodiagnostic imaging and histological studies of angiographically confirmed nidus obliteration. Surg Neurol 37:219–230. https://doi.org/10.1016/0090-3019(92)90235-F
33. Yamamoto M, Jimbo M, Ide M, Lindquist C, Steiner L (1995) Gamma knife radiosurgery in cerebral arteriovenous malformations: postobliteration nidus changes observed on neurodiagnostic imaging. Stereotact Funct Neurosurg 64:126–133. https://doi.org/10.1159/000098772
34. Yamamoto M, Ide M, Jimbo M, Takakura K, Lindquist C, Steiner L (1996) Neuroimaging studies of postobliteration nidus changes in cerebral arteriovenous malformations treated by gamma knife radiosurgery. Surg Neurol 45:110–122. https://doi.org/10.1016/S0090-3019(96)80003-6
35. Yamamoto M, Jimbo M, Hara M, Saito I, Mori K (1996) Gamma knife radiosurgery for arteriovenous malformations: long-term follow-up results focusing on complications occurring more than 5 years after irradiation. Neurosurgery 38:906–914. https://doi.org/10.1097/00006123-199605000-00010
36. Yaşargil MG (1987) Microneurosurgery. Volume IIIA. AVM of the brain, history, embryology, pathological considerations, hemodynamics, diagnostic studies, microsurgical anatomy. Thieme